ChemPubSoc Europe

DOI: 10.1002/ejic.201900894

EurJIC European Journal of Inorganic Chemistry
Full Paper

Check for updates

CO-Releasing Molecules

Wavelength-Dependent Control of the CO Release Kinetics of Manganese(I) Tricarbonyl PhotoCORMs with Benzimidazole Coligands

Ahmed M. Mansour,*[a,b] Christoph Steiger,[c] Christoph Nagel,[b] and Ulrich Schatzschneider[b]

Abstract: A series of photoactivatable CO-releasing molecules (PhotoCORMs) was prepared from manganese pentacarbonyl bromide and 1*H*-benzimidazol-2-ylmethyl-(*N*-phenyl)amine ligands (L) bearing different electron-donating and electron-withdrawing groups R = H, 4-CH_3, 4-OCH_3, 4-Cl, 4-NO_2, 2-, 3-, and 4-$COOCH_3$ on the phenyl substituent to give octahedral manganese(I) complexes of the general formula [$MnBr(CO)_3$(L)]. Aerated DMSO solutions of the compounds are stable in the dark for 16 h with no CO release. However, the compounds rapidly release CO upon illumination at 412–525 nm, depending on the substitution pattern. Its influence on the photophysical and photochemical properties was systematically explored using UV/Vis spectroscopy and CO release measurements with a commercial gas sensor system. In the nitro-substituted compound, the electronically excited state switched from benzimidazole- to phenyl-centered, leading to a markedly different photochemical behavior of this visible-light activated PhotoCORM.

Introduction

In contrast to the well-known general toxicity of high systemic concentrations of carbon monoxide, lower amounts of CO, either enzymatically produced by the activity of heme oxygenase (HO) enzymes on heme, or released from synthetic CO carrier molecules, show surprising beneficial biological effects, including cytoprotection during inflammation, promotion of wound healing, and are also involved in vital signaling processes.[1–4] This has encouraged researchers to explore the administration of CO to humans for potential therapeutic approaches. Unlike the other two small molecule bioregulators (SMBs), nitric oxide and hydrogen sulfide,[5] which interact with a wide range of intracellular targets, including protein sidechains, the chemistry of CO is restricted to coordination to transition metal centers in low oxidation states. As there is a lack of target specificity of CO gas applied to patients by an inhalative delivery system,[6] metal-carbonyl complexes are widely explored as *carbon monoxide-releasing molecules* (CORMs), which act as prodrugs for the delivery of well-controlled quantities of CO to biological systems. Advantages of CORMs include the specific targeting of organs and tissues by tuning of the outer ligand sphere ("drug sphere") without delivering potentially toxic amounts of CO to the whole body. In 2002, Motterlini and co-workers introduced [$Mn_2(CO)_{10}$] (CORM-1) and [$RuCl(\mu\text{-}Cl)(CO)_3]_2$ (CORM-2) as the first CORMs.[7] CORM-1 releases one equivalent of CO upon exposure to UV light, but its low water solubility encouraged the search for more biocompatible metal carbonyl complexes, for example with amino acid auxiliary ligands such as [RuCl(glycinato)$(CO)_3$] (CORM-3).[8] This compound, the most widely studied CORM to date, immediately releases CO upon dissolution in human plasma and exhibits beneficial biological properties such as antimicrobial and anti-inflammatory activity as well as organ preservation effects.[9] The release of CO from the ruthenium coordination sphere is induced by ligand exchange in aqueous medium,[10] but other trigger mechanisms have also been explored, such as changes in pH,[11] redox state,[12] and thermal heating.[13] Furthermore, in so-called *enzyme-triggered CORMs* (ET-CORMs), enzymatic bond cleavage in the ligand periphery induces a series of events finally leading to CO release.[14] In addition, the use of light as an external trigger has enabled facile control of the time, location, and dosage of CO release.[15,16]

Over the last couple of years, the excitation wavelength to trigger *photoactivatable CO-releasing molecules* (PhotoCORMs), has been tuned toward lower energies by proper choice of the coligand system, to ensure deep penetration depth and minimize photodamage to intervening tissue.[17] Manganese(I) tricarbonyl complexes have featured particularly prominent among such systems.[18–22] A wide range of tridentate ligands coordinated to the *fac*-$Mn(CO)_3$ moiety was explored, leading to [$Mn(CO)_3$(tpm)]PF_6 with tpm = tris(pyrazolyl)methane),[18] [$Mn(CO)_3$(tpa-κ^3N)]Br with tpa = tris(2-pyridylmethyl)amine,[19] and [Mn(bpea)$(CO)_3$]PF_6 with bpea = bis(pyrazolyl)methane).[20] While these compounds require photoactivation at 365 nm to trigger the CO release, Mascharak and co-workers improved the

[a] *Department of Chemistry, Faculty of Science, Cairo University, Gamma Street, Giza, Cairo 12613, Egypt*
E-mail: mansour@sci.cu.edu.eg
http://scholar.cu.edu.eg/?q=amansour/
[b] *Institut für Anorganische Chemie, Julius-Maximilians-Universität Würzburg, Am Hubland, 97074 Würzburg, Germany*
[c] *Institut für Pharmazie und Lebensmittelchemie, Julius-Maximilians-Universität Würzburg, Am Hubland, 97074 Würzburg, Germany*
Supporting information and ORCID(s) from the author(s) for this article are available on the WWW under https://doi.org/10.1002/ejic.201900894.

photosensitivity of $[MnBr(CO)_3(pbt)]$ with pbt = 2-(2-pyridyl)-benzothiazole) by increasing the conjugation of the ligand framework.[22] These PhotoCORMs release CO upon illumination at 400–550 nm. The properties of manganese(I) CORMs containing other *N,N*-bidentate ligands with larger conjugated π-system have also been explored, for example in $[MnBr(CO)_3(pmtpm)]$ with pmtpm = 2-pyridyl-*N*-(2′-methylthiophenyl)methyleneimine) and $[MnBr(CO)_3(qmtpm)]$ with qmtpm = 2-quinoline-*N*-(2′-methylthiophenyl)methylene-imine.[23] Some organic drugs such as nifuroxazide, nitazoxanide, and tazarotene have also been used to synthesize new Mn(I) PhotoCORMs, which release CO upon excitation at 468–525 nm.[24]

An important question in the field is the nature of the CO release process, which might either follow a concerted or a step-wise mechanism, as intermediates might have different absorption properties and release kinetics than the original tricarbonyl complex. Kinetic studies on selected compounds by solution IR and EPR spectroscopy as well as quantum chemical calculations revealed the intermediate formation of $Mn(CO)_2$ species upon photolysis, followed by facile oxidation to the Mn(II) and Mn(III) stages in further dark processes.[19,25] Berends and Kurz[25] as well as Schatzschneider[19] found that only one CO ligand is initially photolytically released from the Mn(I) coordination sphere, while the remaining CO molecules require an additional oxidative dark process. Furthermore, in a femtosecond transient absorption UV pump/mid-IR probe spectroscopic study, one CO molecule was photochemically released on very short timescales, but a fraction of the molecules excited was shown to undergo geminate recombination.[26]

In contrast to the excitation wavelength, the CO release kinetics are much more difficult to control by compound design. This is an important bottleneck, as biological effects take place at different timescales, from seconds to hours, and will require a range of PhotoCORMs from fast to slow releasers. For a systematic exploration of the influence of the coligand electron density on the CO release kinetics, a ligand system which allows facile introduction of electron-donating and electron-withdrawing functional groups directly in conjugation with the π-system of the chelating ligand would be highly desirable. Therefore, in the present work, 1*H*-benzimidazol-2-ylmethyl-(*N*-phenyl)amine is introduced as a novel bidentate ligand to the *fac*-$Mn(CO)_3$ moiety. Although the benzimidazole motif is a crucial pharmacophore in drug discovery with interesting biological properties such as antiviral, antitumor, antihistaminic, and antimicrobial activity[27] it has not been extensively explored in the context of CORMs so far. The influence of the type and position of the substituent on the phenyl ring on the photophysical properties of the novel PhotoCORMs was systematically explored and rationalized with the support of DFT calculations.

Results and Discussion

Synthesis of Ligands and Complexes

Eight benzimidazole-based bidentate *N,N*-ligands L^R **1–8** were synthesized by reaction of 2-(chloromethyl)benzimidazole with substituted anilines bearing different functional groups R = H, 4-CH_3, 4-OCH_3, 4-Cl, 4-NO_2, and 2-, 3-, and 4-$COOCH_3$ in the *ortho*-, *meta*-, or *para*-position of the phenyl ring (Scheme 1). They were chosen to study the influence of the type and position of the substituent on the photophysical properties and CO release kinetics of the title compounds. The reaction of ligands **1–8** with manganese(I) pentacarbonyl bromide in acetone at reflux in the dark gave the *fac*-$Mn(CO)_3$ complexes **9–16** in pure form and moderate to good yield (30–73 %).

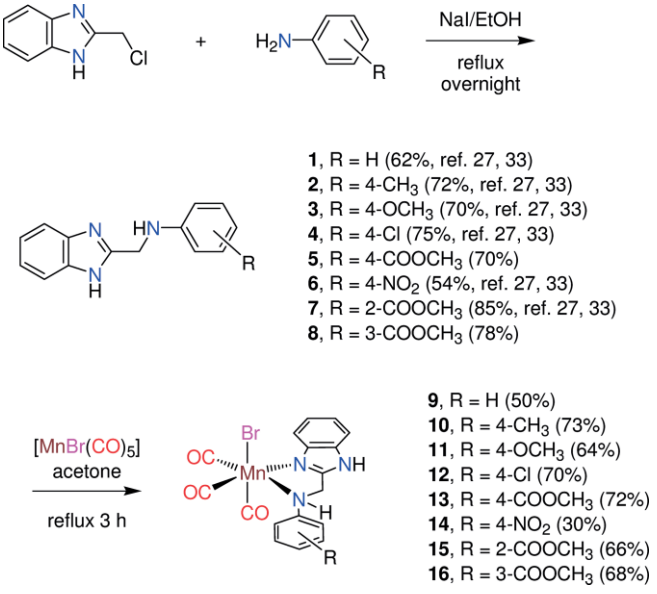

Scheme 1. Synthesis of benzimidazole ligands L^R **1–8** and their manganese(I) tricarbonyl complexes **9–16**.

The IR spectra of ligands **1–8** are characterized by a sharp band around 3345–3450 cm^{-1}, assigned to the N–H-stretching mode of the secondary amino group. The stretching vibrations of the benzimidazole ring could not be identified due to the presence of strong intermolecular hydrogen bonds between the benzimidazole sp^2 nitrogen atom and the benzimidazole NH group.[27] The ν(C=O) vibration of the methyl ester group was found at 1687 (**5**), 1673 (**7**), and 1701 cm^{-1} (**8**), respectively. The IR spectra of complexes **9**, **10**, **12**, and **14** (Figure S1) show three intense ν(C≡O) vibrations at around 2020–2026, 1930, and 1900–1910 cm^{-1} assigned to the symmetrical and two anti-symmetrical stretching modes of the $Mn(CO)_3$ moiety, respectively. The other complexes **11**, **13**, **15**, and **16** display only two bands in the 2020–2030 and 1900–1910 cm^{-1} range, due to the latter one appearing rather broad. Compared to **1–8**, the ν(NH) mode of the amine linker is shifted to lower wavenumbers upon coordination to Mn(I), while the ν(NH) vibration of the benzimidazole cannot be identified due to association of the complexes in the solid-state forming polymeric structure through Br···NH_{bim} contacts as determined by X-ray structure analysis (vide infra). In complex **15**, incorporation of the methyl ester ligand $L^{2-COOCH3}$ (**7**), the C=O group is apparently not involved in the coordination of the Mn(I) center since its stretching mode appears at a higher wavenumber (1688 cm^{-1}) than in the free ligand (1673 cm^{-1}).

In the ^{1}H NMR spectra of ligands **1**–**8**, the benzimidazole NH resonance appears at 12.20–12.46 ppm but is shifted downfield to 13.47–13.58 ppm in complexes **9**–**16**.[27] This is attributed to a change in the electron density on the benzimidazole ring upon metal coordination to the benzimidazole sp^2 nitrogen atom. The triplet signal of the bridging NH group and the doublet of the methylene group in the free ligands (FigureS2) also shift downfield upon coordination to the Mn(I) center. In these metal complexes, the two methylene protons become diastereotopic, giving rise to a pair of doublets between 4.42 and 4.95 ppm (Figure S3).

Crystal Structures

Crystals suitable for X-ray structure analysis were obtained by diffusion of diethyl ether into a solution of the complex in acetone for **9**, **10**, **12**, and **14**. Relevant crystallographic parameters are listed in Table S1 and the molecular structures are shown in Figure 1a–d. Selected bond lengths are presented in Table 1. In all four compounds structurally characterized, the *fac*-Mn(CO)$_3$ moiety is coordinated by the bidentate benzimidazole ligand and a bromide anion to complete the octahedral coordination sphere of the Mn(I) center.

The Mn–N1 bond lengths are 2.122(2), 2.130(2), 2.142(2), and 2.141(2) Å for **9**, **10**, **12** and **14**, respectively. This slight variation is due to the electron-withdrawing effect of the *para*-substituent, 4-Cl (**12**) or 4-NO$_2$ (**14**), or the extended conjugation effect of the methyl group (**10**). As shown in Table 2, the Mn–C bond lengths for the equatorial CO groups are also unequal and longer than the axial one (1.790(2) Å), except for the nitro complex, where the difference is very small. Similar lengths for the Mn1–N2, and Mn1–Br bonds are observed in complexes **9**, **10** and **12**, while the length of the Mn1–Br bond is notably different in the case of **14**.

Table 1. Selected experimental bond lengths (Å) for **9, 10**, **12**, and **14**. For complex **14**, only data for one of two independent molecules with essentially identical metrics in the unit cell is shown.

	9	10	12	14
Mn1–Br	2.542(4)	2.541(4)	2.539(3)	2.5550(4)
Mn1–C1	1.790(3)	1.789(2)	1.790(2)	1.803(2)
Mn1–C2	1.811(3)	1.809(3)	1.806(2)	1.814(2)
Mn1–C3	1.808(2)	1.812(2)	1.814(2)	1.809(2)
Mn1–N1	2.122(2)	2.130(2)	2.142(2)	2.141(2)
Mn1–N2	2.037(2)	2.037(2)	2.034(1)	2.035(2)

Electronic Absorption Spectra and CO-Release Properties

The electronic absorption spectra of **9**–**16** in DMSO show a prominent band centered at around 390 nm with ε_{max} values in the range of 1344–1765 L mol^{-1} cm^{-1} (Figure 2 and Table 2). Compound **15**, with the methyl ester group in the *ortho* position, exhibits an additional intense band at 355 nm with ε_{max} = (2193 ± 93) L mol^{-1} cm^{-1}. The nitro-substituted complex **14** differs from the others as it exhibits only a moderate absorbance at 393 nm but additionally shows an intense broad band at 495 nm, which however strongly changes with incubation for an hour.

Two isosbestic points at 334 and 427 nm are observed during the dark incubation of **14** in DMSO for 1 h. This is attributed to exchange of the axial bromide ligand with solvent, as it is suppressed by bromide addition in some of the other com-

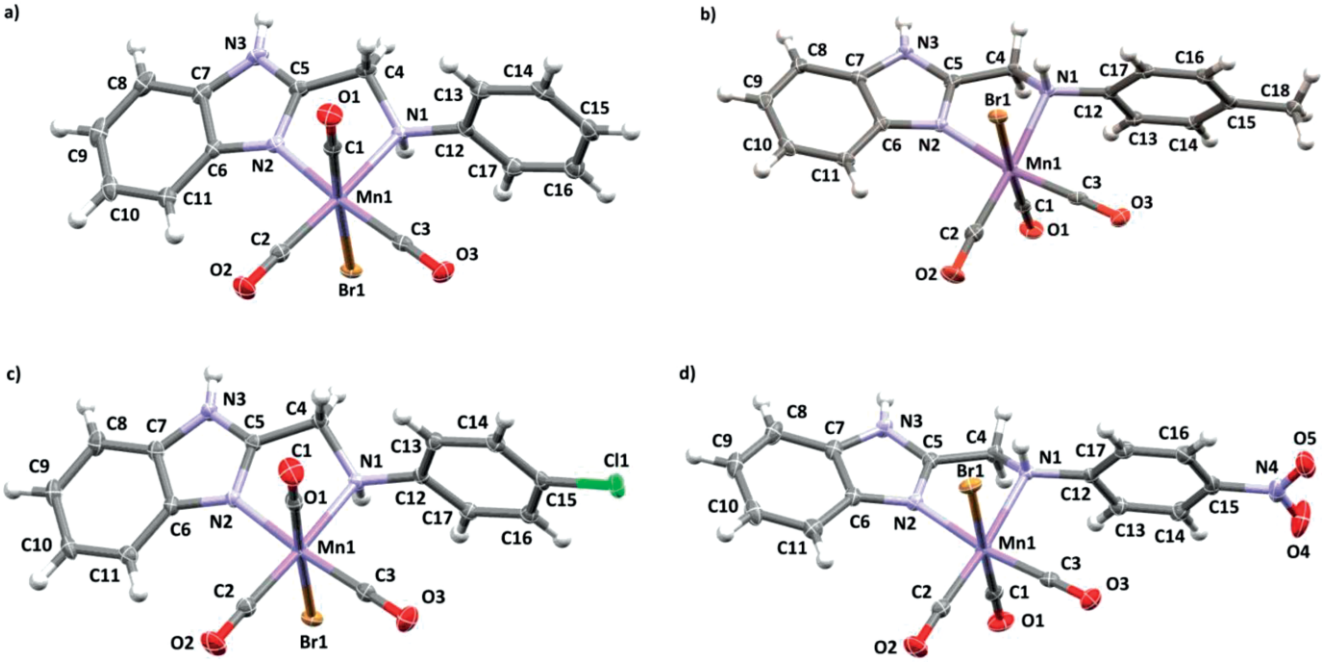

Figure 1. Molecular structures of (a) [MnBr(CO)$_3$(L^H)] **9**, (b) [MnBr(CO)$_3$(L^{4-CH3})] **10**, (c) [MnBr(CO)$_3$(L^{4-Cl})] **12**, and (d) [MnBr(CO)$_3$(L^{4-NO2})] **14**, with ellipsoids drawn at the 50 % probability level. For **14**, only one of two independent molecules with essentially identical metrics in the unit cell is shown.

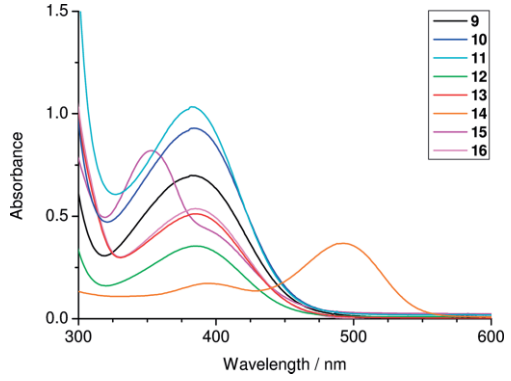

Figure 2. Electronic absorption spectra of complexes **9**–**16** in DMSO [0.27 mM (**9** and **10**); 0.17 mM (**11** and **12**), 0.24 mM (**13**), 0.05 mM (**14**), and 0.38 mM (**15** and **16**)].

Table 2. Absorbance maxima ($\lambda_{max,}$ nm) and molar extinction coefficients ($\varepsilon_{max,}$ L mol^{-1} cm^{-1}) of the lowest energy band in complexes **9**–**16** in DMSO.

	λ_{max}	ε_{max}
9	386	1705 ± 20
10	386	1665 ± 13
11	386	1558 ± 43
12	386	1543 ± 36
13	390	1648 ± 62
14	not determined[a]	
15	355	2193 ± 93
15	395	1344 ± 20
16	386	1765 ± 49

[a] The absorbance of the MLCT band at 495 nm changes with time.

pounds (vide infra). To obtain an insight in the dark stability and photoinduced reactivity profile of **9**–**16**, the complexes were first incubated in DMSO in the dark at room temperature for 16 h and then illuminated with violet or blue light from a LED source at 412 or 468 nm, respectively. Although the illumination wavelength at 468 nm does not coincide with the transition around 390 nm, there is still sufficient absorption at this wavelength. Compound **14** was also exposed to a green LED with an emission maximum at 525 nm, in the flank of the main broad band. In addition, **9**–**16** were also illuminated at 412 nm without previous dark incubation. This allows one to elucidate whether there are additional dark processes such as solvent displacement of the CO and/or bromide ligands from the metal coordination sphere.

When kept in the dark, complexes **9–16** were quite stable for up to 16 h in aerated DMSO solution (Figure S4). Only the three compounds incorporating the electron-donating methyl and methoxy substituents (**10** and **11**) as well as nitro group exhibited a minor change in absorbance over time. This effect is suppressed by addition of an excess of *tert*-butylammonium bromide (Figure S5a) and therefore supports the assignment of the spectral changes observed during dark incubation to exchange of the axial bromido ligand by solvent in these complexes.

Illumination of complex **9**, incorporating the unsubstituted ligand L^H, at 412 nm led to a decrease of the intensity of the band at 386 nm with time and an intermediate state was reached after 25 min. Further illumination resulted in the appearance of a new band at 359 nm, which shifts to 351 nm upon extended exposure to light (Figure 3). Illumination of complexes **10** and **11** (Figure S5b), incorporating the electron-donating methyl and methoxy ligands, at 412 nm had a similar effect. In both cases, a decrease in the intensity of the main absorption band at 386 nm with illumination time was observed while a new band at 361 nm and a shoulder at 309 nm grew in. A plateau value was reached after 75 min of illumination time with no further spectral changes observed after extended illumination.

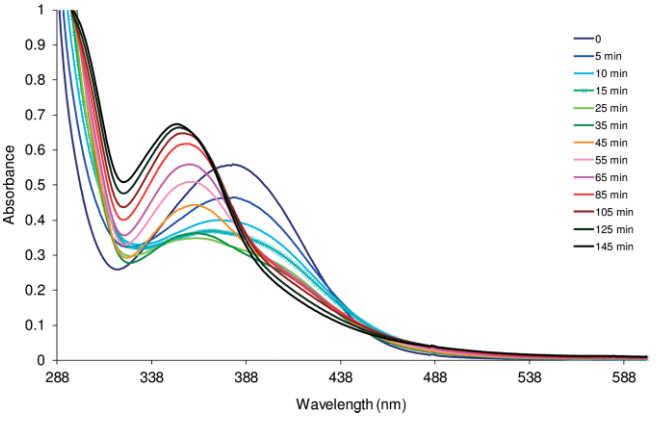

Figure 3. UV/Vis spectral changes of **9** (0.27 mM in DMSO) upon photolysis at 412 nm with increasing illumination time (0–145 min).

When complexes **9**–**12** were illuminated at 468 instead of 412 nm, the decrease of the band at 386 nm was faster and more pronounced than with violet light and only 10–15 min were required to reach the final state (Figure 4). Furthermore, the influence of electron-withdrawing groups in the *para*-, *ortho*- and *meta*-position of the phenyl ring was also studied in the methyl ester compounds **13**, **15**, and **16**. While their dark stability was comparable to **9**, illumination of a pre-incubated sample of **13** at 412 nm (Figure S6) gave rise to a two-step process. The broad band initially observed at 390 nm is first blue-shifted to 359 nm during the initial 5–10 min and then significantly increases in intensity up to 25 min of illumination time without a further shift. Later on, and until the end of the observation time at 80 min, it decreases again (Figure S6). A comparison of spectra acquired under 412 nm illumination with

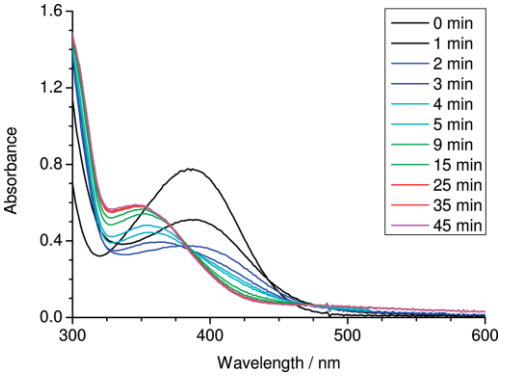

Figure 4. UV/Vis spectral changes of **9** (0.27 mM in DMSO) upon photolysis at 468 nm with increasing illumination time (0–45 min).

and without previous pre-incubation in the dark (Figure S7) indicates that the photoprocess is faster when the solution is first kept in the dark for 16 h. The difference in the photolysis behavior may be attributed to exchange of the axial bromido ligand with DMSO solvent molecules. The latter is harder than the bromide and thus more labilizing, which leads to a faster CO release (Scheme 2). The photolysis profile of **16** at 412 nm is the same as observed for complex **13** (Figure S6).

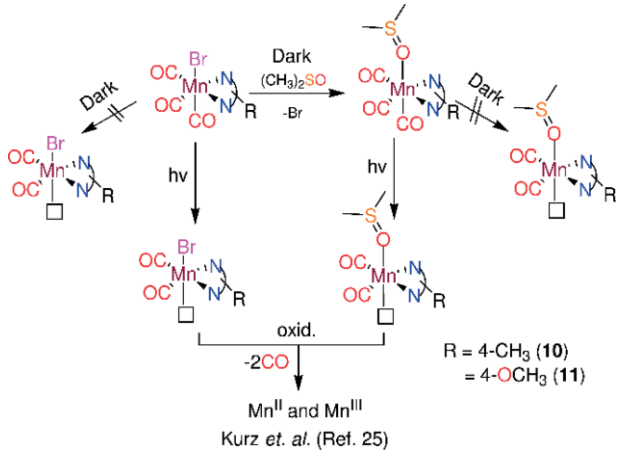

Scheme 2. Illustration of the proposed photoinduced and dark ligand exchange processes.

The electronic absorption spectrum of complex **15**, featuring the methyl ester group in the *ortho*-position of the phenyl ring, shows a dominant band at 355 nm. In contrast to the other compounds, a clear isosbestic point was observed at 372 nm upon illumination at 412 nm (Figure S7). Switching from 412 to 468 nm illumination, the spectral changes observed for **13**, **15**, and **16** resemble those obtained at lower wavelength excitation, but the photolysis process is accelerated (Figure S8). While the 4- and 3-substituted complexes **13** and **16** require 15 and 13 min to reach a plateau level under otherwise identical conditions, the 2-substituted compound **15** reaches this state already after 3 min of illumination at 468 nm.

Finally, the electronic absorption spectrum of a freshly prepared sample of **14** in DMSO is characterized by two bands at 393 and 492 nm. When this complex, incorporating the electron-withdrawing nitro-substituted ligand, is further incubated in the dark for 16 h, two isosbestic points at 334 and 427 nm are observed (Figure S9) and the band at 492 nm decreases with time, while the one at 393 nm increases. When the sample is illuminated at 412 nm after the pre-incubation time, the absorbance at 492 nm decreases while the intensity at 393 nm shows an opposite effect (Figure S10). On the other hand, when a pre-incubated DMSO solution of **14** is exposed to light at 468 nm for 1 min, the intensity of the two bands at 492 and 393 nm both increase (Figure S11). Further illumination, however, leads to a subsequent decrease of the absorbance at 492 nm, accompanied by a red shift to 506 nm.

In contrast to all other compounds discussed in this work, complex **14** also undergoes pronounced spectral changes upon photoactivation at 525 nm (Figure 5). The absorbance of the bands at 492 and 393 nm increases during an initial illumination time of 5 min, but then the former band decreases for the following 55 min. The UV/Vis spectroscopic data on **9–16** reveals the formation of different species during illumination with unique λ_{max} and ε_{max} values, which also depend on whether the compound is first pre-incubated in the dark or immediately exposed to light after dissolution. It is reasonable to assume that the initial dark process is due to exchange of the bromide ligand with solvent while the photoinduced processes are subsequent CO release steps, which also depend on the nature of the axial monodentate ligand (bromide vs. solvent).

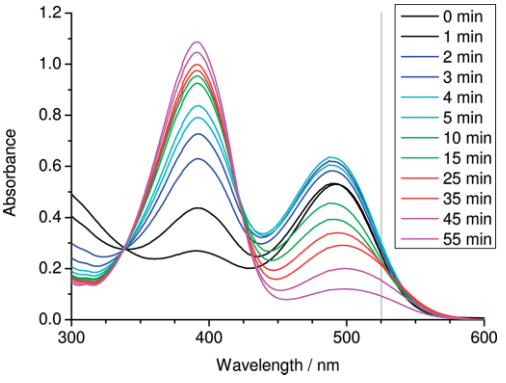

Figure 5. UV/Vis spectral changes of **14** (0.05 mM in DMSO) upon photolysis at 525 nm for 0–55 min without pre-incubation.

Solution IR Spectroscopy

To obtain more detailed information on the composition of the species formed during illumination, solution IR experiments were carried out on **9** and **14** as representative examples. A DMSO solution of PhotoCORM **9** (8 mM) was illuminated in a CaF_2 cell at 468 nm for time intervals of 1 min, after which the light exposure was interrupted to take IR spectra. Before the start of the illumination, the IR spectrum of **9** shows three bands at 2021, 1923, and 1906 cm^{-1}, which are assigned to the symmetrical and antisymmetrical CO stretches of the *fac*-$Mn(CO)_3$ moiety. During the illumination, the latter modes disappear while two new bands grow in at 1968 and 1862 cm^{-1} (Fig. S12), which are assigned to the formation of a dicarbonyl species. The stability of **14** was investigated by IR spectroscopy. The IR spectrum of **14** shows three strong bands at 2023, 1927 and 1907 cm^{-1} (Fig. S13), which slightly shift upon dark incubation in DMSO. However, this mostly affects the two lower energy antisymmetrical stretching vibrations while the other bands remain unchanged. No evidence of the formation of dicarbonyl species or a *fac* to *mer* isomerization process was observed,[19,20] as the formation of a dicarbonyl species would give rise to only two bands at lower wavenumbers, while the *mer*-isomer normally exhibits CO stretching modes at higher values relative to the *fac* species.

CO Release Studies Using a Sensor Chip System

Due to the complicated photoprocesses occurring in most of the compounds and the difficulties associated with the myo-

globin assay, such as reducing conditions due to the presence of a large amount of dithionite, the CO scavenging properties of the heme protein, which might shift the CO release equilibrium, and potential spectral overlap of the metal complex and protein absorbances, CO release from compounds **9**–**16** dissolved in a mixture of water and DMSO (10:1 v/v) was studied with a commercial gas sensor upon illumination at 468 nm (Figure 6). Under these conditions, all compounds showed rather similar release profiles and reached a plateau valued after about 30 min of exposure to 468 nm light. In the case of the *para*-nitro compound **14**, 525 nm photoexcitation was also investigated. The compound initially showed a slow and linear CO release when triggered at this wavelength, but after 4 h of extended illumination, also reached a plateau value (Figure 6). About 0.9–1.8 equivalents of CO are released from **9–16** upon illumination for 30–40 min at 468 nm. In contrast, at 525 nm excitation of **14**, only 0.9 CO equivalents are detected. This opens up the interesting prospect of actually controlling the release kinetics by selection of the excitation wavelength, depending on whether the biological process of interest requires a fast or slow CO release, without the need to prepare fast and slow CO releasers separately. Other visible-light inducible Mn(I) tricarbonyl PhotoCORMs bearing *N*,*N*-bidentate ligands such as 2-(2-pyridyl) benzothiazole (λ_{ex} = 400 nm, DMSO/H_2O, $t_{1/2}$ = 4.3 min),[23] *N*,*N*′-bis(2,6-diisopropylphenyl)-1,4-diaza-1,3-butadiene (λ_{ex} = 560 nm, DMSO/H_2O, $t_{1/2}$ = 35 min),[28] and 2-phenylazopyridine derivatives (λ_{ex} ≥ 625 nm, CH_2Cl_2, $t_{1/2}$ = 3.5 h) exhibit widely divergent half-life times of CO release.[29]

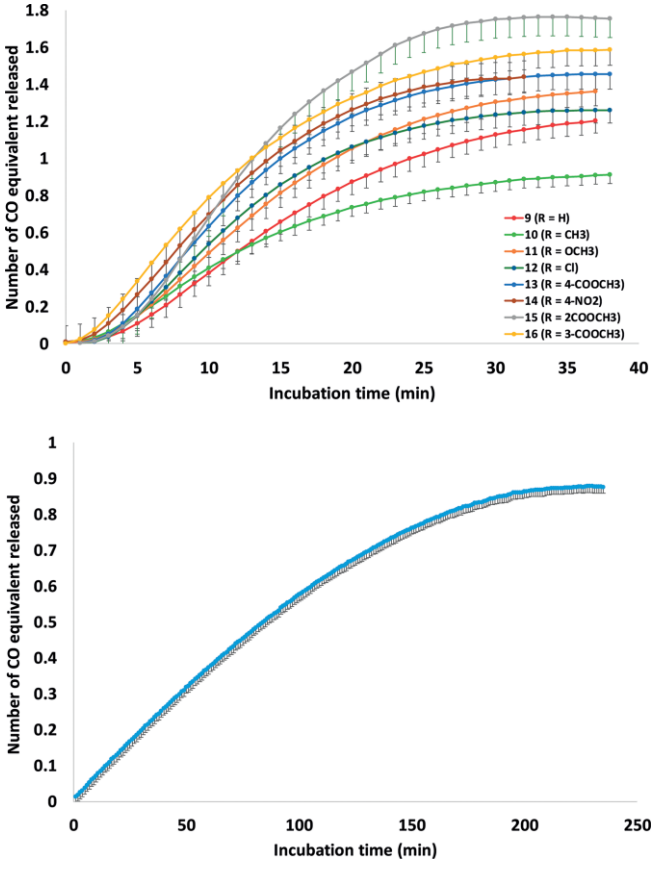

Figure 6. CO release profiles of **9**–**16** in DMSO/water (1:10 v/v) analyzed with a commercial CO sensor system under constant illumination with LED light at 468 or 525 nm (top) during the initial 30 min and (bottom) upon extended illumination of **14** at 525 nm for up to 4 h. All data are expressed as mean ± SD (n = 3).

DFT and TDDFT Calculations

To obtain an insight in the structural and electronic features of the title compounds, in particular those that were not characterized by X-ray structure analysis, the structures of **9**–**16** were optimized by DFT using the BP86 functional and a TZVP basis set and showed a good match of bond parameters and vibrational bond positions with experimental values (Tables S2 and S3).[19,20,30] For an additional insight in the electronic structure and assignment of the most relevant UV/Vis transitions, TDDFT calculations were carried out on **9** and **14** to obtain the 45 lowest-energy spin-allowed singlet excitations (Table 3). While both compounds **9** and **14** exhibit some closely spaced states at around 260–300 nm (Table 3 and Table S4), the nature of the first relevant lowest energy state (state 1 in the case of **9** and state 3 in the case of **14**) is markedly different (Figure 7). In the unsubstituted parent compound **9**, the difference density plot reveals a shift from the metal to the benzimidazole part of the bidentate ligand and the transition is thus of MLCT character. On the other hand, in the case of the nitro-substituted compound **14**, the transition also originates from the manganese center, but leads to a build-up of electron density on the nitrophenyl group of the ligand system upon excitation. Thus, by variation of the substituent on the phenyl ring, the transition is switched from benzimidazole- to phenyl-centered. This is as-

Table 3. Energies (in nm), oscillator strength (f_{osc}), main orbital contributions, and type of transitions involved in the most important singlet excitations for **9** and **14** calculated with TDDFT using the B3LYP functional and a TZVP basis set.

Compound **9**				
State[a]	λ	f_{osc}	main transitions[b]	type of transition[c]
1	361	0.0351	109→110 (90 %)	MLCT Mn→bim
2	324	0.0139	108→110 (30 %) 109→111 (45 %)	MLCT Mn→im/CO
8	290	0.0183	108→111 (25 %) 109→112 (34 %)	MLCT Mn→phenyl/CO
10	273	0.0216	108→114 (54 %)	MLCT Mn→ phenyl/CO
13	264	0.0127	106→110 (32 %) 109→115 (55 %)	MLCT Mn→bim
Compound **14**				
State[a]	λ	f_{osc}	main transitions[b]	type of transition[c]
3	653	0.0161	118→121 (99 %)	MLCT Mn→phenyl
6	358	0.0312	120→122 (92 %)	MLCT Mn→bim
7	335	0.0215	120→123 (70 %)	MLCT Mn→phenyl/CO
16[d]	299	0.0217	119→123 (42 %)	MLCT Mn→phenyl/CO
17[d]	351	0.0573	114→121 (66 %)	LLCT Br→phenyl
21	279	0.2646	112→121 (52 %)	MLCT Mn→phenyl/CO LLCT NO_2→phenyl/CO
22	273	0.1875	112→121 (24 %)	MLCT Mn→phenyl/CO LLCT NO_2→phenyl/CO

[a] Only strong transitions with an oscillator strength > 0.01 in the 250–800 nm range are reported. [b] Only contributions >20 % are listed. [c] Bim = benzimidazole and im = imidazole. [d] The reversed order is due to state 16 experiencing a smaller solvent shift than most of the others.

sumed to be the origin of the markedly different photochemical behavior of the two compounds.

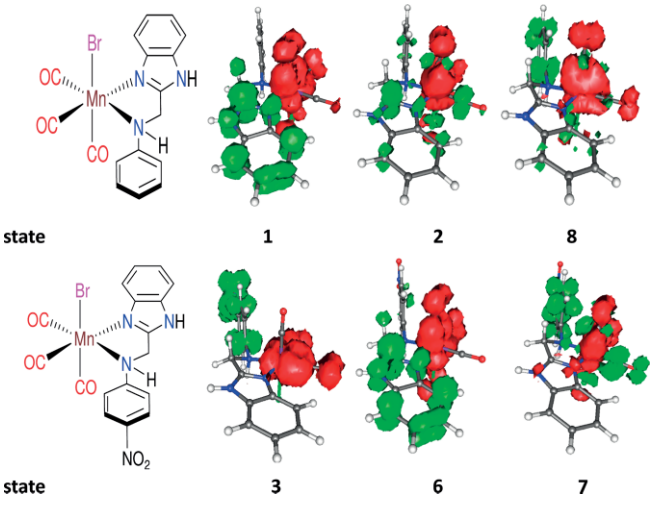

Figure 7. TDDFT difference density plots for the most important singlet excitations of **9** and **14** in the 290 to 660 nm range. Isosurface values are plotted at ±0.002, with positive values shown in green and negative ones in red.

Conclusions

Eight manganese(I) carbonyl complexes of the general formula $[MnBr(CO)_3(L)]$ incorporating 1*H*-benzimidazol-2-ylmethyl-(*N*-phenyl)amine derivatives as the chelating ligand L were synthesized and characterized, including X-ray analysis for four of the compounds. Different electron-withdrawing and electron-donating substituents in the 2-, 3-, and 4-position of the phenyl ring were introduced to study their influence on the photophysical properties of the title compounds. All of them do not release CO in aerated DMSO for up to 16 h upon incubation in the dark, but the presence of electron-donating substituents facilitates axial bromide substitution by solvent, which can however be suppressed by addition of an excess of bromide salt. The electronic absorbance spectrum of the nitro-substituted compound features a broad band at 495 nm with a tail extending to 550 nm while the other complexes show the lowest energy band at around 385 nm. With the aid of TDDFT calculations, these differences can be traced by to the nature of the MLCT state, which is from the manganese center to the benzimidazole part of the ligand in the non-substituted compound, but to the nitrophenyl group in the complex with the strongly electron-withdrawing functionality. Photoinduced spectral changes depend on whether the compound is first pre-incubated in the dark or a freshly prepared solution directly illuminated. This may be assigned to axial bromide exchange with solvent in the pre-incubated samples. Thus, in addition to the functional groups in the ligand periphery, also the axial ligand on the metal center has an important influence on the CO release process. Carbon monoxide release from the title compounds was studied with a sensor chip system at different excitation wavelengths to avoid difficulties associated with the myoglobin assay. All title complexes showed a rather similar release profile and reached plateau values after about 30 min of exposure to 468 nm light. The nitro-substituted compound could also be activated with green light at 525 nm. Under these conditions, an initial slow and linear increase in CO concentration was observed. Only after extended illumination for 4 h, a plateau value was reached for this complex, albeit with a lower CO release efficiency. In summary, by variation of the peripheral substituent on the phenyl ring in this series of PhotoCORMs, green light photoactivation was achieved with a strongly electron-withdrawing nitro group, and the release kinetics were controlled by choice of the activation wavelength. This opens up the opportunity to switch a compound from slow to fast CO releaser by simple variation of the light source, depending on the biological process to be investigated.

Experimental Section

General procedures

Reactions were carried out in oven-dried Schlenk glassware under an atmosphere of pure argon and exclusion of light using degassed solvents. All the chemicals were purchased from commercial sources and used as received. Elemental analysis was carried out using an Elementar Vario Micro Cube CHN analyzer. IR spectra were recorded in the solid state on a Nicolet 380 FT-IR spectrometer equipped with a smart iFTR accessory. UV/Vis spectra were measured using an Agilent 8453 diode array spectrophotometer. NMR spectra were recorded on a Bruker Avance 500 spectrometer (^{1}H: 500.13 MHz, ^{13}C{^{1}H}: 125.77 MHz) at ambient temperature. Chemical shifts δ in ppm indicate a downfield shift relative to TMS and are referenced relative to the residual proton signal of the solvent.[31] Coupling constants *J* are given in Hertz (Hz). Peak multiplicities are indicated as singlet (s), doublet (d), doublet of doublet (dd), triplet (t), and multiplet (m), respectively. Electrospray ionization (ESI) mass spectra were recorded in negative ion mode using a Bruker micrOTOF spectrometer with a solvent flow rate of 4 μL min^{-1}. Only the most abundant peak of each isotope distribution is given. The illumination was carried out with custom-built LED light sources, 412 nm (King-bright Elec. Co., model YDG-504VC, part no. 181000–05), 468 nm (King-bright Elec. Co., 5000 m cd, part. no. BL0106–15–299) and 525 nm (King-bright Elec. Co., 6500 m cd, part. no. L-34ZGC). Ferrioxalate actinometry was used to determine the photon flux of the light sources used.[32] It was found to be 6.69×10^{-10}, 1.25×10^{-9}, and 6.69×10^{-11} Einstein s^{-1} for the 412, 468 and 525 nm LED source light, respectively.

Synthetic procedures

Synthesis of benzimidazole ligands 1–8. The benzimidazole ligands (L^H (**1**), L^{4-CH3} (**2**), L^{4-OCH3} (**3**), L^{4-Cl} (**4**), L^{4-NO2} (**6**), and $L^{2-COOCH3}$ (**7**)) were prepared as previously reported.[27,33] The new compounds $L^{4-COOCH3}$ (**5**) and $L^{3-COOCH3}$ (**8**) were synthesized as follows: a solution of 2-chloromethyl benzimidazole (1.66 g, 10 mmol) and methyl-4-aminobenzoate (1.51 g, 10 mmol for $L^{4-COOCH3}$ (**5**)) or methyl-3-aminobenzoate (1.51 g, 10 mmol for $L^{3-COOCH3}$ (**8**)) in ethanol (30 mL) was heated to reflux overnight in the presence of sodium iodide (1.50 g, 10 mmol). The solvent was then partially removed under reduced pressure and the resulting precipitate was separated after dilution with water. Compounds **5** and **8** were then recrystallized from a mixture of ethanol and water (50:50 v/v).

$L^{4-COOCH3}$ 5. Yellow solid yield 70 % (1.97 g, 7.0 mmol). IR (ATR, cm^{-1}): $\tilde{\nu}$ = 3357 (s, NH), 1687 (s, C=O). ^{1}H NMR (500.13 MHz, [D$_6$]DMSO, ppm): δ = 12.31 (s, 1H, bim-N*H*), 7.68 (d, 2H, ^3J = 8.7 Hz,

phenyl-H3/5), 7.47 (m, 2H, bim-H4/7), 7.16 (t, 1H, ^3J = 5.7 Hz, CH_2NH), 7.11 (m, 2H, bim-H5/6), 6.68 (d, 2H, ^3J = 8.9 Hz, phenyl-H2/6), 4.54 (d, 2H, ^3J = 5.8 Hz, CH_2NH), 3.71 (s, 3H, $COOCH_3$). ^{13}C NMR (125.75 MHz, [D$_6$]DMSO, ppm): δ = 166.3 ($COOCH_3$), 152.6 (bim-C2), 152.5 (phenyl-C1), 130.9 (phenyl-C3/5), 121.3–121.6 (bim-C4/5/6/7), 116.6 (phenyl-C4), 111.5 (phenyl-C2/6), 51.3 (CH_3), 41.1 (CH_2). $C_{16}H_{15}N_3O_2$: C 68.30, H 5.37, N 14.97; found C 66.96, H 5.80, N 15.08.

L$^{3-COOCH3}$ 8. White solid, yield 78 % (2.20 g, 7.8 mmol). IR (ATR, cm^{-1}): $\tilde{\nu}$ = 3371 (s, NH), 1701 (s, C=O). ^{1}H NMR (500.13 MHz, [D$_6$]DMSO, ppm): δ = 12.29 (s, 1H, bim-N*H*), 7.47 (m, 2H, bim-H4/7), 7.25 (s, 1H, phenyl-H2), 7.20–7.15 (m, 2H, phenyl-H5/6), 7.11 (m, 2H, bim-H5,6), 6.89 (d, 1H, ^3J = 7.5 Hz, phenyl-H4), 6.65 (t, 1H, CH_2NH, ^3J = 5.7 Hz), 4.51 (d, 2H, ^3J = 5.8 Hz, CH_2NH), 3.77 (s, 3H, $COOCH_3$). ^{13}C-NMR (125.75 MHz, [D$_6$]DMSO, ppm): δ = 166.3 ($COOCH_3$), 153.2 (bim-C2), 148.5 (phenyl-C1), 130.3 (bim-C3a/7a and phenyl-C3), 129.2 (phenyl-C6), 121.3–121.4 (bim-C4/5/6/7), 117.1 (phenyl-C5), 116.7 (phenyl-C4), 112.8 (phenyl-C2), 52.0 ($COOCH_3$), 41.6 (CH_2NH). $C_{16}H_{15}N_3O_2$: C 68.30, H 5.37, N 14.97; found C 68.17, H 5.43, N 15.10.

Synthesis of manganese(I) tricarbonyl complexes 9–16. The benzimidazole ligand (L^H, 80 mg; L^{4-CH3}, 85 mg; L^{4-OCH3}, 91 mg; L^{4-Cl}, 93 mg; L$^{4-COOCH3}$, 101 mg; L^{4-NO2}, 96 mg; L$^{2-COOCH3}$, 101 mg; L$^{3-COOCH3}$, 101 mg; 0.36 mmol each) and manganese pentacarbonyl bromide (100 mg, 0.36 mmol) were dissolved under argon in degassed anhydrous acetone (20 mL) and heated to reflux for 3 h while protected from light by wrapping the apparatus in aluminium foil. The solution was then left in the dark for slow evaporation down to 5 mL, whereupon a precipitate formed which was filtered off, washed with *n*-hexane and dried under vacuum for 5 d. Crystals suitable for X-ray structure analysis were obtained by diffusion of diethyl ether into a solution of the complex in acetone.

[MnBr(CO)$_3$(L^H)] 9. Orange crystals yield 50 % (80 mg, 0.18 mmol). IR (ATR, cm^{-1}): $\tilde{\nu}$ = 3182 (w, NH), 2020 (vs, C≡O), 1928 (vs, C≡O), 1905 (vs, C≡O), 1598, 1477, 1432, 1213, 1053. ^{1}H NMR (500.13 MHz, [D$_6$]DMSO, ppm): δ = 13.47 (s, 1H, bim-N*H*), 7.79 (m, 1H, bim-H7), 7.69 (m, 1H, bim-H4), 7.62 (m, 1H, CH_2NH), 7.52 (m, 1H, phenyl-C6), 7.39 (m, 2H, bim-H5/6), 7.34 (m,1H, phenyl-H4), 7.18 (m, 2H, phenyl-H3/5), 7.07–7.16 (m, 1H, phenyl-H2), 4.71–4.56 (m, 2H, CH_2NH). ^{13}C NMR (125.75 MHz, [D$_6$]DMSO, ppm): δ = 226.2 (C≡O), 222.1 (C≡O), 221.8 (C≡O), 157.1 (bim-C2), 152.5 (phenyl-C1), 142.2 (bim-C7a), 135.7 (bim-C3a), 130.1 (phenyl-C4), 125.4 (phenyl-C2), 124.5 (bim-C6), 124.1 (bim-C5), 121.0 (phenyl-C6), 119.2 (phenyl-C3/5), 117.3 (bim-C7), 113.9 (bim-C4), 50.9 (CH_2NH). MS (ESI$^-$, acetone): *m/z* 355.952 [M – H – 3CO]$^-$, 439.940 [M – H]$^-$, 521.866 [M + Br]$^-$. $C_{17}H_{13}BrMnN_3O_3$: C 46.18, H 2.96, N 9.50; found 46.54, H 2.93, N, 9.52.

[MnBr(CO)$_3$(L^{4-CH3})] 10. Yellow powder yield 73 % (120 mg, 0.26 mmol). IR (ATR, cm^{-1}): $\tilde{\nu}$ = 3217 (w, NH), 2023 (vs, C≡O), 1929 (vs, C≡O), 1902 (vs, C≡O), 1595, 1476, 1446, 1276, 1064. ^{1}H NMR (500.13 MHz, [D$_6$]DMSO, ppm): δ = 13.55 (s, 1H, bim-N*H*), 7.79 (m, 1H, bim-H7), 7.67 (m, 1H, bim-H4), 7.45 (m, 1H, phenyl-H6), 7.35 (m, 2H, bim-H5/6), 7.17 (m, 1H, phenyl-H2), 7.07–7.13 (m, 3H, CH_2NH and phenyl-H3/5), 4.53–4.67 (m, 2H, CH_2NH), 2.22 (s, 3H, CH_3). ^{13}C-NMR (125.75 MHz, [D$_6$]DMSO, ppm): δ = 225.0 (C≡O), 221.1 (C≡O), 220.7 (C≡O), 156.0 (bim-C2), 149.0 (phenyl-C1), 141.1 (bim-C7a), 134.7 (bim-C3a), 133.2 (phenyl-C4), 129.5 (phenyl-C6), 129.2 (phenyl-C2), 123.5 (bim-C6), 123.2 (bim-C5), 119.9 (phenyl-C5), 118.1 (phenyl-C3), 116.3 (bim-C7), 112.8 (bim-C4), 49.8 (CH_2NH), 20.1 ($COOCH_3$). MS (ESI$^-$, acetone): *m/z* 369.972 [M – H – 3CO]$^-$, 453.959 [M – H]$^-$, 535.884 [M + Br]$^-$. $C_{18}H_{15}BrMnN_3O_3$: C 47.39, H 3.31, N 9.21; found 47.03, H 3.33, N, 9.22.

[MnBr(CO)$_3$(L^{4-OCH3})] 11. Orange powder yield 64 % (108 mg, 0.23 mmol). IR (ATR, cm^{-1}): $\tilde{\nu}$ = 3194 (w, NH), 2022 (vs, C≡O), 1907 (vs, C≡O), 1597, 1510, 1474, 1434, 1254, 1077. ^{1}H NMR (500.13 MHz, [D$_6$]DMSO, ppm): δ = 13.54 (s, 1H, bim-N*H*), 7.80 (m, 1H, bim-H7), 7.69 (m, 1H, bim-H4), 7.52 (m, 1H, Phenyl-H6), 7.40 (m, 2H, bim-H5/6), 7.15 (m, 1H, phenyl-H2), 6.93–6.99 (m, 3H, CH_2NH and phenyl-H3/5), 4.67–4.51 (m, 2H, CH_2NH), 3.07 (s, 3H, OCH_3). ^{13}C NMR (125.75 MHz, [D$_6$]DMSO, ppm): δ = 225.1 (C≡O), 221.4 (C≡O), 220.9 (C≡O), 156.1 (phenyl-C1), 155.9 (bim-C2), 144.2 (phenyl-C4), 141.1 (bim-C7a), 134.7 (bim-C3a), 123.6 (bim-C6), 123.2 (bim-C5), 121.2 (phenyl-C6), 119.5 (phenyl-C2), 116.4 (bim-C7), 114.3 (bim-C3/5), 113.0 (bim-C4), 55.3 ($COOCH_3$), 50.4 (CH_2NH), MS (ESI$^-$, acetone): *m/z* 385.962 [M – H – 3CO]$^-$, 469.950 [M – H]$^-$, 551.877 [M + Br]$^-$. $C_{18}H_{15}BrMnN_3O_4$: C 45.79, H 3.20, N 8.90; found 45.64, H 3.35, N, 8.64.

[MnBr(CO)$_3$(L^{4-Cl})] 12. Orange crystals yield 70 % (120 mg, 0.25 mmol). IR (ATR, cm^{-1}): $\tilde{\nu}$ = 3212 (w, NH), 2022 (vs, C≡O), 1932 (vs, C≡O), 1903 (vs, C≡O), 1592, 1478, 1436, 1221, 1056. ^{1}H NMR (500.13 MHz, [D$_6$]DMSO, ppm): δ = 13.58 (s, 1H, bim-N*H*), 7.78 (m, 2H, bim-C7/phenyl-H3), 7.67 (m, 1H, bim-C4), 7.46 (m, 2H, phenyl-H2/6), 7.39 (m, 3H, CH_2NH, bim-H5/6), 7.18 (m, 2H, and phenyl-H3/5), 4.67–4.53 (m, 2H, CH_2NH). ^{13}C NMR (125.75 MHz, [D$_6$]DMSO, ppm): δ = 225.1 (C≡O), 220.9 (C≡O), 220.7 (C≡O), 155.8 (bim-C2), 150.6 (phenyl-C1), 141.2 (bim-C7a), 134.7 (bim-C3a), 129.1 (phenyl-C4), 128.7 (phenyl-C6), 128.2 (phenyl-C2), 123.5 (bim-C6), 123.3 (bim-C5), 121.9 (phenyl-C5), 119.9 (phenyl-C3), 116.3 (bim-C7), 113.0 (bim-C4), 49.5 (CH_2NH). MS (ESI$^-$, acetone): *m/z* 389.928 [M – H – 3CO]$^-$, 473.888 [M – H]$^-$, 555.828 [M + Br]. $C_{17}H_{12}BrClMnN_3O_3$: C 42.84, H 2.54, N 8.82; found 43.44, H 2.95, N, 8.68.

[MnBr(CO)$_3$(L$^{4-COOCH3}$)] 13. Red powder yield 72 % (130 mg, 0.26 mmol). IR (ATR, cm^{-1}): $\tilde{\nu}$ = 3202 (m, NH), 2025 (vs, C≡O), 1904 (vs, C≡O), 1697 (m, C=O), 1606, 1432, 1285, 1182, 1114. ^{1}H NMR (500.13 MHz, [D$_6$]DMSO, ppm): δ = 13.56 (s, 1H, bim-N*H*), 7.93 (m, 2H, phenyl-H2/6), 7.79 (m, 1H, bim-H7), 7.70 (m, 1H, bim-H4), 7.55 (m, 1H, bim-H3), 7.41 (m, 2H, bim-H5/6), 7.26 (m, 1H, phenyl-H5), 7.13 (t, 1H, ^3J = 5.8 Hz, CH_2NH), 4.57–4.75 (m, 2H, CH_2NH), 3.80 (s, 3H, $COOCH_3$), ^{13}C NMR (125.75 MHz, [D$_6$]DMSO, ppm): δ = 225.3 (C≡O), 220.7 (C≡O), 220.6 (C≡O),165.5 ($COOCH_3$), 155.8 (bim-C2), 152.1 (phenyl-C1), 141.2 (bim-C7a), 134.8 (bim-C3a), 130.6 (phenyl-C6), 130.1 (phenyl-C2), 125.4 (phenyl-C4), 123.6 (bim-C6), 123.3 (bim-C5), 120.2 (phenyl-C3), 118.4 (phenyl-C5), 116.3 (bim-C7), 113.0 (bim-C4), 52.0 ($COOCH_3$), 49.0 (CH_2NH). MS (ESI$^-$, acetone): *m/z*: 413.935 [M – H – 3CO]$^-$, 497.935 [M – H]$^-$. $C_{19}H_{15}BrMnN_3O_5$: C 45.62, H 3.02, N 8.40; found 45.17, H 3.27, N, 8.05.

[MnBr(CO)$_3$(L^{4-NO2})] 14. Orange powder yield 30 % (53 mg, 0.11 mmol). IR (ATR, cm^{-1}): $\tilde{\nu}$ = 3180 (w, NH), 2026 (vs, C≡O), 1950 (vs, C≡O), 1906 (vs, C≡O), 1595, 1526 (s, NO_2), 1478, 1342 (s, NO_2), 1228. ^{1}H NMR (500.13 MHz, [D$_6$]DMSO, ppm): δ = 13.60 (s, 1H, bim-N*H*), 8.39 (s, 1H, CH_2NH), 8.25 (m, 2H, phenyl-H3/5), 7.77 (m,1H, bim-H7), 7.71 (m,1H, bim-H4), 7.41 (m, 2H, bim-H5/6), 7.35 (m, 1H, phenyl-H6), 7.14 (m, 1H, phenyl-H2), 4.75–4.64 (m, 2H, CH_2NH). ^{13}C NMR (125.75 MHz, [D$_6$]DMSO, ppm): δ = 225.5 (C≡O), 220.7 (C≡O), 220.5 (C≡O), 157.6 (phenyl-C4), 155.7 (bim-C2), 154.2 (phenyl-C1), 141.2 (bim-C7a), 134.8 (bim-C3a), 126.0 (phenyl-C5), 125.3 (phenyl-C3), 123.8 (bim-C6), 123.4 (bim-C5), 121.6 (phenyl-C6), 119.0 (phenyl-C2), 116.3 (bim-C7), 113.1 (bim-C4), 49.0 (CH_2NH). MS (ESI$^-$, acetone): *m/z* 400.917 [M – H – 3CO]$^-$, 484.904 [M – H]$^-$. $C_{17}H_{12}BrMnN_4O_5$: C 41.91, H 2.48, N 11.50; found 41.79, H 2.61, N, 11.20.

[MnBr(CO)$_3$(L$^{2-COOCH3}$)] 15. Yellow crystals yield 66 % (120 mg, 0.24 mmol). IR (ATR, cm^{-1}): $\tilde{\nu}$ = 3173 (w, NH), 2029 (vs, C≡O), 1911 (vs, C≡O), 1688 (m, C=O), 1604, 1493, 1448, 1268, 1096. ^{1}H NMR (500.13 MHz, [D$_6$]DMSO, ppm): δ = 13.54 (s, 1H, bim-N*H*), 8.85 (m, 1H, CH_2NH), 8.01 (m, 1H, phenyl-H6), 7.80 (s, 1H, bim-H7), 7.70 (s,

1H, bim-H4), 7.57 (m, 1H, phenyl-H5), 7.42 (m, 2H, bim-H5/6), 7.11 (m, 1H, phenyl-H3), 6.93 (m, 1H, phenyl-H5), 4.42–4.95 (m, 2H, CH_2NH), 3.96 (s, 3H, COOCH_3). ^{13}C NMR (125.75 MHz, [D_6]DMSO, ppm): δ = 225.6 (C≡O), 220.7 (C≡O), 219.9 (C≡O), 167.0 (*C*OOCH$_3$), 156.9 (bim-C2), 154.3 (phenyl-C1), 141.3 (bim-C7a), 135.2 (phenyl-C5), 134.7 (bim-C3a), 130.6 (phenyl-C2), 123.7 (bim-C6), 123.2 (bim-C5), 120.0 (phenyl-C4), 121.1 (phenyl-C3), 116.3 (phenyl-C6), 116.1 (bim-C7), 113.2 (bim-C4), 52.6 (COO*C*H$_3$), 50.7 (*C*H$_2$NH). MS (ESI$^-$, acetone): *m/z* 413.936 [M – H – 3CO]$^-$, 497.930 [M – H]$^-$. $C_{19}H_{15}BrMnN_3O_5$: C 45.62, H 3.02, N 8.40; found 45.46, H 3.08, N, 8.40.

[MnBr(CO)$_3$(L$^{3-COOCH3}$)] 16. Orange powder yield 68 % (120 mg, 0.24 mmol). IR (ATR, cm^{-1}): $\tilde{\nu}$ = 3201 (m, NH), 2025 (vs, C≡O), 1904 (vs, C≡O), 1696 (m, C=O), 1607, 1426, 1289, 1184, 1058. ^{1}H NMR (500.13 MHz, [D_6]DMSO, ppm): δ = 13.58 (s, 1H, bim-N*H*), 8.04 (m, 1H, phenyl-H6), 7.94 (m, 1H, phenyl-H4), 7.78 (m, 1H, bim-H7), 7.70 (m, 1H, bim-H4), 7.55 (m, 1H, phenyl-H3), 7.39 (m, 2H, bim-H5/6), 7.26 (m, 1H, phenyl-H2), 7.11 (m, 1H, CH$_2$N*H*), 4.72–4.59 (m, 2H, CH_2NH), 3.80 (s, 3H, COOCH_3). ^{13}C NMR (125.75 MHz, [D_6]DMSO, ppm): δ = 225.1 (C≡O), 220.8 (C≡O), 220.766 (C≡O), 165.1 (*C*OOCH$_3$), 155.8 (bim-C2), 152.2 (phenyl-C1), 141.1 (bim-C7a), 134.7 (bim-C3a), 130.1 (phenyl-C2), 125.4 (phenyl-C4), 123.6 (bim-C6), 123.3 (bim-C5), 120.2 (phenyl-C3), 118.3 (phenyl-C5), 116.3 (bim-C7), 113.0 (bim-C4), 52.1 (COO*C*H$_3$), 49.1 (*C*H$_2$NH). MS (ESI$^-$, acetone): *m/z* 413.942 [M – H – 3CO]$^-$, 497.930 [M – H]$^-$. $C_{19}H_{15}BrMnN_3O_5$: C 45.62, H 3.02, N 8.40; found 45.55, H 3.36, N, 8.31.

X-ray crystallography

A single crystal of **9**, **10**, **12**, or **14** was immersed in a film of perfluoropolyether oil, mounted on a glass fiber and transferred to a stream of cold nitrogen of the diffractometer. Diffraction data were collected on a Bruker x8 Apex II diffractometer with multi-layer mirror graphite monochromated *Mo-K*$_\alpha$ radiation (λ = 0.71073 Å) at 100 K. The final cell constants were obtained from a least square fit of a subset of a few thousand strong reflections. The program CrysAlis CCD was used for data collection. CrysAlis RED and CrysAlis CCD software were used for cell refinements and data reduction. The program SADABS was used to account for the absorption.[34] The OLEX2 program was used for refinement and artwork of the structure.[35] All the hydrogen atoms were included in the calculated positions.

CCDC 1552459 (for **9**), 1552460 (for **10**), 1552461 (for **12**), and 1552462 (for **14**) contain the supplementary crystallographic data for this paper. These data can be obtained free of charge from The Cambridge Crystallographic Data Centre.

Density functional theory calculations

The density functional theory calculations were carried out on the Linux cluster of the Leibniz-Rechenzentrum (LRZ) in Munich using ORCA version 2.8,[36] with the BP86 functional combined with the resolution-of-the-identity (RI) approximation, a def2-TZVP/def2-TZVP/J basis set,[30] the tightscf and grid4 options and the COSMO solvation model with DMSO as the solvent. The starting geometries for the optimization runs were constructed based on the available crystallographic data. The resulting geometries were characterized as local minima via harmonic frequency analysis, showing the absence of imaginary modes. The electronic transitions were calculated by TDDFT with the B3LYP functional and the RIJCOX keyword using the same level of theory as for the optimizations. The first 45 singlet excited states were calculated (nroots 45). Graphics were created with gOpenmol.

CO release studies using a sensor chip system

The CO release profiles were recorded in a custom-made measurement cell consisting of two DN25 flanges (bottom closed, Rettberg, Göttingen, Germany) equipped with a XXS CO probe from Dräger (Lübeck, Germany).[37,38] The probe was connected to an X-am 5000 gas sensor (Dräger). Of each compound, 0.6 mg were weighted on a XP 56 microbalance (Mettler Toledo, Columbus, OH), dissolved in DMSO (1 mL) and then mixed with water (10 mL). Of this solution, 4 mL were transferred to the measurement cell within 1 h at the latest and stirred at 140 rpm (Variomag Telesystem, Thermo Scientific, MA). The photoinduced CO release was examined by illuminated at 468 or 525 nm. The light source was placed in a distance of 3.0 cm laterally to the measurement cell. Readouts were corrected proportionally to the exact mass as well as the molar amount of each compound.

Acknowledgments

The stay of A. M. Mansour in Germany was supported by a German-Egyptian Research Short-Term Scholarship (GERSS) from the Deutscher Akademischer Austauschdienst (DAAD) and a Georg Forster Fellowship from the Alexander von Humboldt Foundation (AvH). Wolfgang Obert from the Electronics Workshop of the Institut für Anorganische Chemie, Universität Würzburg, is acknowledged for the expert construction of the LED light sources. Thanks also to Prof. Dr. Lorenz Meinel for access to the electrochemical CO sensor system.

Keywords: CO-releasing molecules (CORMs) · Manganese Carbonyl ligands · Benzimidazole · TDDFT

[1] a) R. Tenhunen, H. S. Marver, R. Schmid, *Proc. Natl. Acad. Sci. USA* **1968**, *61*, 748; b) M. D. Maines, *Annu. Rev. Pharmacol.* **1997**, *37*, 517.
[2] H. P. Kim, S. W. Ryter, A. M. K. Choi, *Ann. Rev. Pharmacol. Toxicol.* **2006**, *46*, 411.
[3] A. Nakao, D. J. Kaczorowski, R. Sugimoto, T. R. Billiar, K. R. McCurry, *J. Clin. Biochem. Nutr.* **2008**, *42*, 78.
[4] a) L. Wu, R. Wang, *Pharmacol. Rev.* **2005**, *57*, 585; S. W. Ryter, J. Alam, A. M. K. Choi, *Physiol. Rev.* **2006**, *86*, 583.
[5] C. Szabo, *Sci. Transl. Med.* **2010**, *2*, 1.
[6] U. Schatzschneider, *Br. J. Pharmacol.* **2015**, *172*, 1638; C. C. Romao, W. A. Blättler, J. D. Seixas, G. J. L. Bernardes, *Chem. Soc. Rev.* **2012**, *41*, 3571.
[7] R. Motterlini, J. Clark, R. Foresti, P. Sarathchandra, B. Mann, C. Green, *Circ. Res.* **2002**, *90*, E17.
[8] J. E. Clark, P. Naughton, S. Shurey, C. J. Green, T. R. Johnson, B. E. Mann, R. Foresti, R. Motterlini, *Circ. Res.* **2003**, *93*, 2e.
[9] M. Desmard, K. S. Davidge, O. Bouvet, D. Morin, D. Roux, R. Foresti, J. D. Ricard, E. Denamur, R. K. Poole, P. Montravers, R. Motterlini, J. Boczkowski, *FASEB J.* **2009**, *23*, 1023; P. Urquhart, G. Rosignoli, D. Cooper, R. Motterlini, M. Perretti, *J. Pharmacol. Exp. Ther.* **2007**, *321*, 656.
[10] T. R. Johnson, B. E. Mann, I. P. Teasdale, H. Adams, R. Foresti, C. J. Green, R. Motterlini, *Dalton Trans.* **2007**, 1500.
[11] F. Zobi, A. Degonda, M. C. Schaub, A. Y. Bogdanova, *Inorg. Chem.* **2010**, *49*, 7313.
[12] B. J. Aucott, J. S. Ward, S. G. Andrew, J. Milani, A. C. Whitwood, J. M. Lynam, A. Parkin, I. J. S. Fairlamb, *Inorg. Chem.* **2017**, *56*, 5431.
[13] P. C. Kunz, H. Meyer, J. Barthel, S. Sollazzo, A. M. Schmidt, C. Janiak, *Chem. Commun.* **2013**, *49*, 4896.
[14] a) E. Stamellou, D. Storz, S. Botov, E. Ntasis, J. Wedel, S. Sollazzo, B. K. Kraemer, W. Van-Son, M. Seelen, H. G. Schmalz, *Redox Biol.* **2014**, *2*, 739; b) S. Romanski, E. Stamellou, J. T. Jaraba, D. Storz, B. K. Kraemer, M. Hafner, S. Amslinger, H. G. Schmalz, B. A. Yard, *Free Radical Biol. Med.* **2013**, *65*, 78.
[15] R. D. Rimmer, H. Richter, P. C. Ford, *Inorg. Chem.* **2010**, *49*, 1180.
[16] F. Mohr, J. Niesel, U. Schatzschneider, C. W. Lehmann, *Z. Anorg. Allg. Chem.* **2012**, *638*, 543.

[17] S. L. Hopkins, B. Siewert, S. H. C. Askes, P. Veldhuizen, R. Zwier, M. Heger, S. Bonnet, *Photochem. Photobiol. Sci.* **2016**, *15*, 644.
[18] J. Niesel, A. Pinto, H. W. Peindy N'Dongo, I. Merz, I. Ott, R. Gust, U. Schatzschneider, *Chem. Commun.* **2008**, 1798.
[19] C. Nagel, S. Mclean, R. K. Poole, H. Braunschweig, T. Kramer, U. Schatzschneider, *Dalton Trans.* **2014**, *43*, 9986.
[20] S. Pai, M. Hafftlang, G. Tongo, C. Nagel, J. Niesel, S. Botov, H. G. Schmalz, B. Yard, U. Schatzschneider, *Dalton Trans.* **2014**, *43*, 8664.
[21] M. A. Gonzalez, M. A. Yim, S. Cheng, A. Moyes, A. J. Hobbs, P. K. Mascharak, *Inorg. Chem.* **2012**, *51*, 601.
[22] M. A. Gonzalez, S. J. Carrington, N. L. Fry, J. L. Martinez, P. K. Mascharak, *Inorg. Chem.* **2012**, *51*, 11930.
[23] S. J. Carrington, I. Chakraborty, J. M. L. Bernard, P. K. Mascharak, *ACS Med. Chem. Lett.* **2014**, *5*, 1324.
[24] A. M. Mansour, *J. Photochem. Photobiol. A* **2017**, *335*, 78; A. M. Mansour, O. R. Shehab, *J. Organomet. Chem.* **2016**, *822*, 91.
[25] U. Sachs, G. Schaper, D. Winkler, D. Kratzert, P. Kurz, *Dalton Trans.* **2016**, *45*, 17464; H. M. Berends, P. Kurz, *Inorg. Chim. Acta* **2012**, *380*, 141.
[26] P. Rudolf, F. Kanal, J. Knorr, C. Nagel, J. Niesel, T. Brixner, U. Schatzschneider, P. Nürnberger, *J. Phys. Chem. Lett.* **2013**, *4*, 596.
[27] N. T. Abdel-Ghani, A. M. Mansour, *Eur. J. Med. Chem.* **2012**, *47*, 399; N. T. Abdel-Ghani, A. M. Mansour, *Inorg. Chim. Acta* **2011**, *373*, 249.
[28] V. Yempally, S. J. Kyran, R. K. Raju, W. Y. Fan, E. N. Brothers, D. J. Darensbourg, A. A. Bengali, *Inorg. Chem.* **2014**, *53*, 4081.
[29] E. Kottelat, A. Ruggi, F. Zobi, *Dalton Trans.* **2016**, *45*, 6920.
[30] a) A. Schaefer, H. Horn, R. Ahlrichs, *J. Chem. Phys.* **1992**, *97*, 2571; b) F. Weigend, R. Ahlrichs, *Phys. Chem. Chem. Phys.* **2005**, *7*, 3297.
[31] G. R. Fulmer, A. J. M. Miller, N. H. Sherden, H. E. Gottlieb, A. Nudelman, B. M. Stoltz, J. E. Bercaw, K. I. Goldberg, *Organometallics* **2010**, *29*, 2176.
[32] C. Bischof, T. Joshi, A. Dimri, L. Spiccia, U. Schatzschneider, *Inorg. Chem.* **2013**, *52*, 9297.
[33] N. T. Abdel-Ghani, A. M. Mansour, *J. Mol. Struct.* **2011**, *991*, 108; N. T. Abdel-Ghani, A. M. Mansour, *Spectrochim. Acta Part A* **2011**, *81*, 529; N. T. Abdel-Ghani, A. M. Mansour, *Spectrochim. Acta Part A* **2012**, *86*, 605; *Spectrochim. Acta A* **2012**, *91*, 272.
[34] G. M. Sheldrick, *Universität Göttingen*, Germany, **2006**.
[35] O. V. Dolomanov, L. J. Bourhis, R. J. Gildea, J. A. K. Howard, H. Puschmann, *J. Appl. Crystallogr.* **2009**, *42*, 339.
[36] F. Neese, *WIREs Comput. Mol. Sci.* **2011**, *2*, 73–78.
[37] C. Steiger, K. Uchiyama, T. Takagi, K. Mizushima, Y. Higashimura, M. Gutmann, S. Botov, H. G. Schmalz, Y. Naito, L. Meinel, *J. Controlled Release* **2016**, *239*, 128.
[38] C. Steiger, T. Lühmann, L. Meinel, *J. Controlled Release* **2014**, *189*, 46.

Received: August 20, 2019

CO-Releasing Molecules

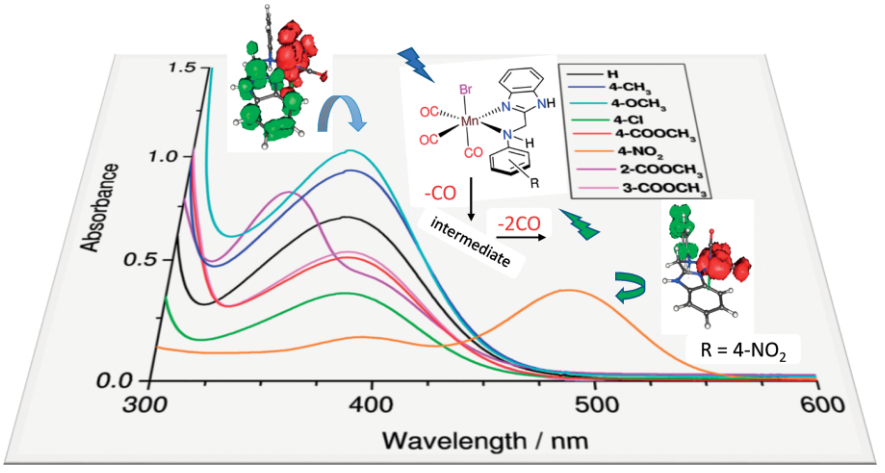

The influence of coligand electron density on the CO release was systematically explored in a series of manganese tricarbonyl complexes with benzimidazole ligands bearing electron-donating and withdrawing functional groups in direct conjugation with the ligand π system.

DOI: 10.1002/ejic.201900894